DEVELOPMENTAL DYNAMICS 236:1650–1662, 2007

Runx2 Is Essential for Larval Hyobranchial Cartilage Formation in *Xenopus laevis*

Ryan Kerney,[1]* Joshua B. Gross,[2] and James Hanken[1]

The vertebrate transcription factor protein Runx2 is regarded as a "master regulator" of bone formation due to the dramatic loss of the osseous skeleton in the mouse homozygous knockout. However, *Runx2* mRNA also is expressed in the pre-hypertrophic cartilaginous skeleton of the mouse and chicken, where its developmental function is largely unknown. Several tiers of *Runx2* regulation exist in the mouse, any of which may account for its seeming biological inactivity during early stages of skeletogenesis. Unlike mouse and chicken, zebrafish require Runx2 function in early cartilage differentiation. The present study reveals that the earlier functional role of Runx2 in cartilage differentiation is shared between zebrafish and *Xenopus*. A combination of morpholino oligonucleotide injections and neural crest transplants indicate that Runx2 is involved in differentiation of the cartilaginous hyobranchial skeleton in the frog, *Xenopus laevis*. Additionally, in situ hybridizations show runx2 mRNA expression in mesenchymal precursors of the cartilaginous skull, which reveals the earliest pre-patterning of these cartilages described to date. The early distribution of runx2 resolves the homology of the larval suprarostral plate, which is one of the oldest controversies of anuran skull development. Together these data reveal a shift in Runx2 protein function during vertebrate evolution towards its exclusive roles in cartilage hypertrophy and bone differentiation within the amniote lineage. *Developmental Dynamics 236:1650–1662, 2007.* © 2007 Wiley-Liss, Inc.

Key words: *Xenopus laevis;* Runx2; cartilage formation; suprarostral; Pipidae; evolution

Accepted 30 March 2007

INTRODUCTION

The runt-domain-containing transcription factor Runx2 (also known as Aml3, Cbfa1, Osf2, Pebp2alphaA, Pebp2, and Sl3-3 enhancer factor 1) is critical in osteoblast differentiation and chondrocyte maturation in amniotes. The homozygous *Runx2* knockout mouse is notable for its complete loss of bone (Komori et al., 1997) and mutations in its coding sequence result in the human autosomal dominant disorder cleidocranial dysplasia, in which several dermal bones are reduced or absent (Mundlos et al., 1997). The function of Runx2 in determining the osteoblast cell lineage is in opposition to the role of the chondrocyte regulator Sox9. Osteoblasts and chondrocytes that express *Runx2* mRNA are daughter cells of the *Sox9*-expressing lineage in mouse (Mori-Akiyama et al., 2003), and overexpression of either transcription factor can drive the differentiation of progenitor cells towards cartilage or bone in vivo (Ueta et al., 2001; Eames et al., 2004). Whereas runx2 is known to be expressed in mature osteocytes in the adult frog, *Xenopus laevis* (Moriishi et al., 2005), little attention has been given to its expression or function during earlier stages of anuran development.

Runx2 belongs to a family of transcription factors collectively called the runx genes. Three vertebrate paralogs, derived from a triplication of an ancestral runx (Levanon et al., 2003; Glusman et al., 2004), share the highly conserved DNA-binding "runt" domain. While Runx2 is of primary importance in bone development (Banerjee et al., 1997; Ducy et al., 1997; Komori et al., 1997; Otto et al., 1997), *Runx1* and *3* are also expressed in the developing skeleton (Yamashiro et al., 2002; Lian et al., 2003; Smith et al., 2005) suggesting some functional redundancy between these family members (Cameron et al., 2003;

[1]Museum of Comparative Zoology, Harvard University, Cambridge, Massachusetts
[2]Harvard Medical School, Department of Genetics, Boston, Massachusetts
Grant sponsor: NSF Amphibia Tree; Grant number: EF-0334846; Grant sponsor: NIH Genetics and Genomics Training Grant; Grant sponsor: Sigma-Xi Grant in Aid of Research.
***Correspondence to: Museum of Comparative Zoology, Harvard University 26 Oxford St., Cambridge, MA 02138.**
E-mail: kerney@fas.harvard.edu

DOI 10.1002/dvdy.21175
Published online 1 May 2007 in Wiley InterScience (www.interscience.wiley.com).

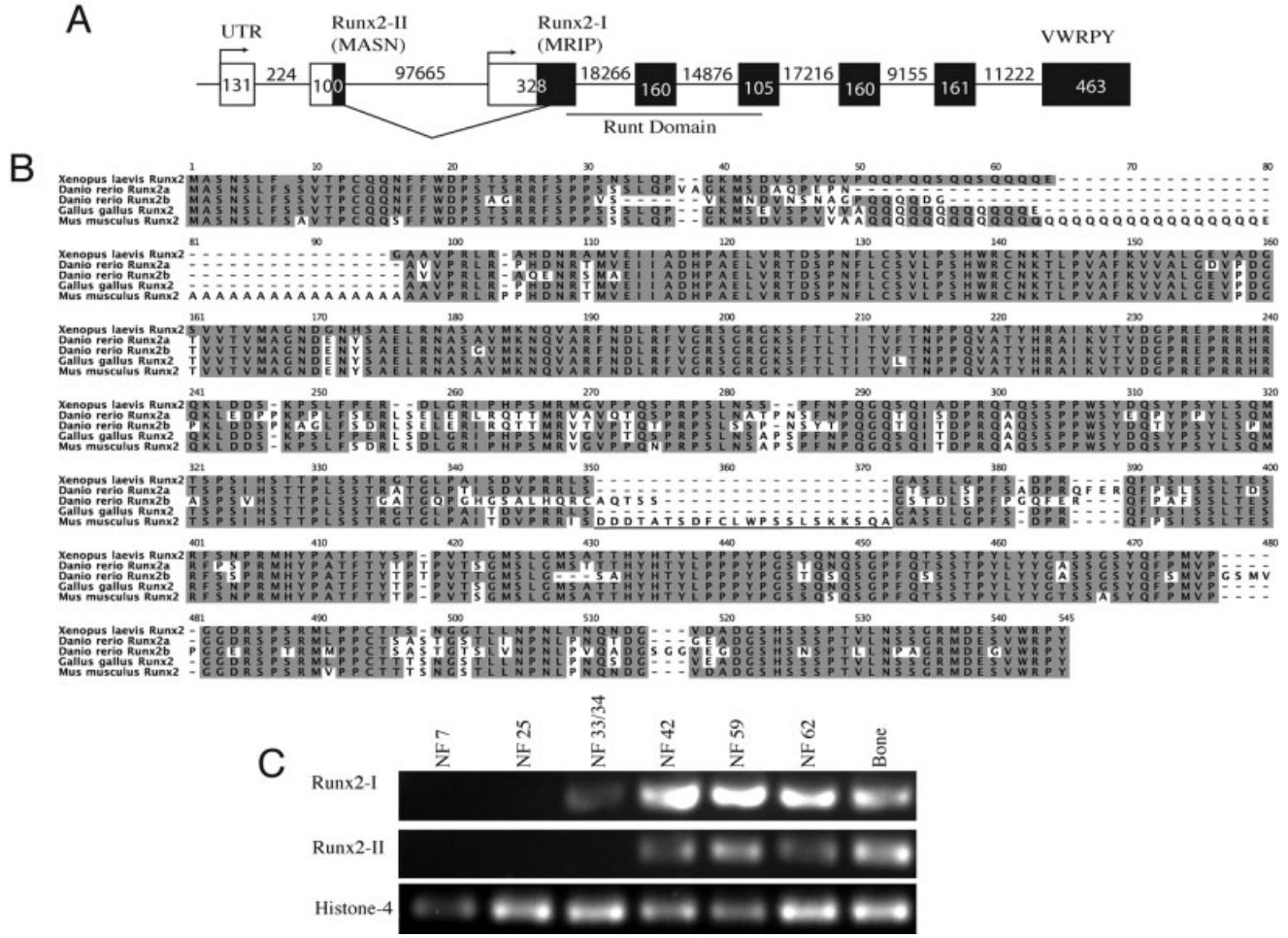

Fig. 1. *Xenopus laevis* runx2 structure and expression. **A:** Exon distribution based on a pairwise Blast with the *Xenopus tropicalis* scaffold 328 (Joint Genome Institute). Exon lengths (bp) are shown inside boxes; intron lengths are shown above lines. Hollow boxes denote untranslated regions (UTR's), and filled boxes indicate protein-coding sequences. The two isoforms vary in their 5′ UTR through the first few coding bases. They begin with the amino acid sequences MRIP (runx2-I) and MASN (runx2-II). The majority of the coding region is shared between both isoforms. All known runx proteins end with the conserved amino acid sequence VWRPY. Introns are not distributed to scale. **B:** Protein alignment of runx2-II among *Xenopus laevis, Danio rerio* (zebrafish), *Gallus gallus* (domestic chicken), and *Mus musculus* (mouse). Two versions of the runx2 gene are found in *Danio*, each with two separate isoforms. The 22–amino acid transactivation domain (underlined) found in mouse is not shared with other vertebrates. Amino acids shared with the *Xenopus* sequence are highlighted in grey. Dashed lines indicate gaps. **C:** RT-PCR analysis of the separate isoforms in various Nieuwkoop and Faber (NF) stages and tissues. Runx2-I appears by stage 33/34 and remains transcriptionally active through metamorphosis (stage 62), whereas runx2-II appears later (stage 42). Both transcripts are found in the froglet long bone. Histone-4 RT-PCR, used as a positive control, was expressed throughout development.

Flores et al., 2006). Overexpression and RNA interference of mouse Runx1 has revealed its role in early cartilage formation (Wang et al., 2005). However, Runx1 is not involved in zebrafish cartilage formation, where Runx2 appears to have taken over the functional role in chondrogenesis (Flores et al., 2006). Runx family members interact with core binding factor beta (also known as Cbfb, Pea2, Pebp2, Pebp2b, Pebpb2), which increases their transcriptional activity (Speck and Dzierzak, 2001; Kundu et al., 2002). All three runx genes have a variable amino terminus, which is derived from two separate isoforms. These are under the control of two separate promoters, which vary in the first few amino acids. In all runx genes, the type II isoform begins with the amino acid sequence MASN, whereas the type I isoform begins with the amino acid sequence MRIP (Cameron et al., 2003; Rennert et al., 2003; Ito, 2004; Blyth et al., 2005). In *Runx2*, these isoforms show temporal and spatial variation in expression (Choi et al., 2002; Lengner et al., 2002; Stock and Otto, 2005), and selective knockouts of individual isoforms indicate unique developmental roles for type I and type II RUNX2 (Harada et al., 1999; Choi et al., 2002).

In amniotes, *Runx2* mRNA is present in mesenchymal precursors of osteoblasts and in those chondrocytes fated to be replaced by bone (Inada et al., 1999; Enomoto et al., 2000; Enomoto-Iwamoto et al., 2001; Iwamoto et al., 2003; Eames et al., 2004). Its early expression in chondrocytes does not appear to have any functional role until later stages of cartilage hypertrophy and osteogenesis (Kim et al., 1999; Ueta et al., 2001). During early stages of cartilage differentiation, the mature protein may be suppressed by

Fig. 2. In situ hybridizations of runx2 and sox9 in the mandibular neural crest stream. **A:** Anterior views of the head showing the distribution of both transcripts over several developmental stages. Runx2 mRNA expression is first apparent in the pre-chondrogenic suprarostral plate (SP) by stage 31. Additional expression appears in the cranial trabeculae (CT) by stage 35/36 (see Fig. 3). This expression is in a subset of the mandibular arch crest (MA), which expresses sox9. The expression of sox9 mRNA is progressively restricted to co-localize with runx2. By stage 39, both transcripts overlap in the presumptive suprarostal plate (SP). The expression of runx2 decreases in the suprarostral plate by stage 41, although some expression persists in the palatoquadrate anlagen (PQ). Sox9 expression in the suprarostral plate is fused in the midline by stage 41, with continued expression in the palatoquadrate and new expression in the infrarostral (IR) and Meckel's cartilages (MC). **B:** Ventral views of stage 39 embryos stained with runx2 and sox9. The cement gland has been removed with a scalpel. Both transcripts are expressed in the future ceratohyal (CH) and palatoquadrate cartilages. The latter is clearly divided into a posterior sub-ocular arc (SA) and anterior quadratocranial commissure (QC), which connects to the suprarostral plate dorsally. There is a small flange of staining off of the palatoquadrate in both preparations that reveals the future Meckel's cartilage (asterisk).

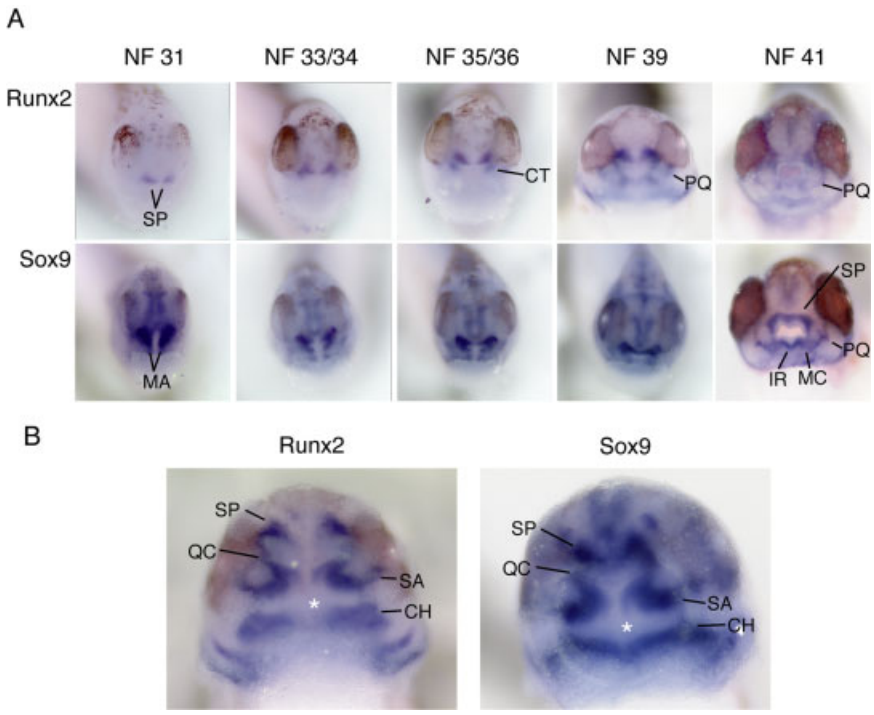

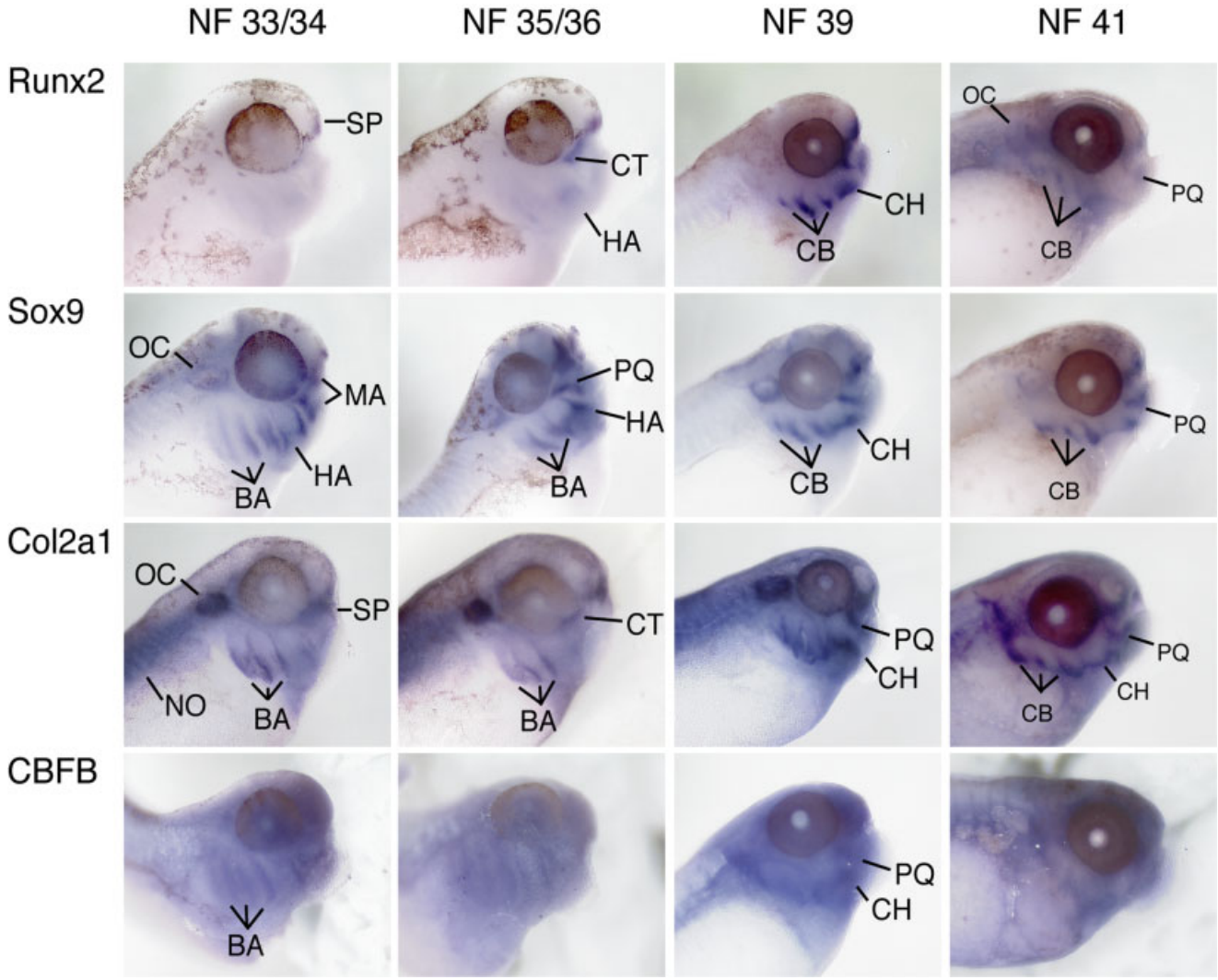

Fig. 3.

any of several levels of regulation, including splice variation, ubiquitination, acetylation, and phosphorylation, as well as functional control through various DNA binding partners and inhibitors (reviewed in Franceschi and Xiao, 2003; Iwamoto et al., 2003; Bae and Lee, 2005; Lengner et al., 2005; Goldring et al., 2006).

Zebrafish have two copies of many genes, including runx2 (Flores et al., 2004; van der Meulen et al., 2005). Early suppression of runx2a function does not affect early cartilage formation. However, the zebrafish *runx2b* paralog, which is strongly expressed in precursors of the pharyngeal arch cartilages, is essential for pharyngeal cartilage formation (Flores et al., 2006). This developmental role of *runx2b* differs from the amniote model, and may indicate a replacement of runx1 function in zebrafish cartilage formation. The present study will describe the early distribution and function of two runx2 isoforms in *Xenopus laevis*, and will compare its early role in hyobranchial cartilage formation to zebrafish and amniote models.

RESULTS

Xenopus laevis Runx2 Gene Structure

Xenopus runx2 genomic structure was determined by a pairwise BLAST comparison of the full-length *Xenopus laevis* runx2 cDNA, which was cloned in this study, against the *Xenopus tropicalis* scaffold 328 (Joint Genome Institute, Walnut Creek, CA). The gene consists of eight exons and seven introns ranging in size from 9 to 91 Kb (Fig. 1A). The presence of two isoforms beginning with amino acids MASN (type II) and MRIP (type I) is conserved in all vertebrate runt-domain genes examined to date. The order of appearance, from 5′ to 3′, of the first MASN isoform open reading frame followed by an intron, which is then followed by the MRIP open reading frame, is also shared with other vertebrate runt-domain genes (Fig. 1A).

The *Xenopus laevis* Runx2-I protein shares 83% amino acid sequence identity with *Mus musculus* RUNX2-I, and 81 and 70% identity with *Danio rerio* Runx2a-I and Runx2b-I, respectively. The *Xenopus* protein has a short poly-glutamine/alanine repeat region with only ten glutamine residues and two alanines (Fig. 1B). These repeat sequences are longer in the chicken, mouse, and human orthologs of the gene. The high ratio of glutamine to alanine in *Xenopus* may indicate a relatively higher level of Runx2 transcriptional activity (Fondon and Garner, 2004). *Xenopus*, zebrafish, and chicken sequences lack a 22–amino acid stretch found in the mouse sequence beginning with the amino acid sequence DDTAT (underlined in Fig. 1B). This region is a transactivation domain in mammals (Thirunavukkarusu et al., 1998), but it is not found in any orthologs outside of the mammalian RUNX2.

Runx2 Expression

Tissue-specific, reverse-transcription PCR of the two isoforms shows the temporal distribution of the runx2 transcripts during embryonic development (Fig. 1C). The runx2-I isoform is transcriptionally active by stage 33/34, which is before the histological differentiation of any skeletal anlagen in the developing embryo (Nieuwkoop and Faber, 1994). The runx2-II isoform is transcriptionally active by stage 42. Its later expression correlates with the formation of cartilaginous extracellular matrix in the palatoquadrate, ceratohyal, and basihyal, the first three cartilages to form during embryonic development (stage 42; Nieuwkoop and Faber, 1994). However, this stage-specific RT-PCR analysis does not rule out earlier expression of runx2-II between stages 33/34 and 42. Similar expression differences between these two isoforms are found in the mouse, where *Runx2-I* also is expressed earlier than *Runx2-II* (Stock and Otto, 2005). Both isoforms continue to be expressed through metamorphosis.

Anti-runx2 in situ hybridizations were performed with a probe that targets a region of the runx2 gene, which is conserved between the two isoforms and includes the 3′ untranslated region (UTR). Isoform-specific probes were not made, as the two sequences differ in only a few amino acids on their 5′ ends. Based on the RT-PCR results, the distribution of runx2 during early stages (up to and including stage 33/34) indicates expression of the runx2-I isoform. Staining between stages 33/34 and 41 may represent the distribution of either isoform.

Runx2 expression first appears during stage 31 in two small regions of the anterior head dorsal to the stomodeum (Fig. 2A). This staining pattern coincides with the future location of the larval suprarostral plate (Trueb and Hanken, 1992; Seufert et al., 1994), and is similar to the anterior anlagen of the suprarostral cartilages described for *Rana temporaria* (Spemann, 1898). These paired stains are separate from the presumptive cranial trabeculae, which do not express runx2 until stage 35/36. By stage 39, the cranial trabeculae anlagen fuse to the precursors of the suprarostral plate, which have expanded towards the midline (Fig. 2A).

Early sox9 staining within the mandibular crest stream overlaps anterior runx2 staining in stage-31 embryos. Sox9 mRNA expression in the mandibular arch subsequently shrinks

Fig. 3. In situ hybridizations of runx2, sox9, collagen2a1, and cbfb. All images are lateral views, anterior to the right. Runx2 expression begins in the presumptive suprarostral plate (SP). It expands to the anlage of the cranial trabeculae (CT) and a faint portion of the hyoid arch crest (HA) by stage 35/36. Runx2 staining includes the future ceratobranchial (CB) and ceratohyal (CH) cartilages by stage 39, and is additionally found in the otic capsule (OC) by stage 41. The expression of runx2 in the ceratohyal decreases during stage 41 as this element begins to chondrify. The distribution of sox9 is more extensive than that of runx2 by stage 33/34, with strong expression in the mandibular (MA), hyoid (HA), and branchial (BA) arch neural crest streams. Its expression in the crest becomes restricted by stage 35/36 with a clear distribution in the precursors of the future palatoquadrate and continued expression in the hyoid and branchial arches. By stage 39, both runx2 and sox9 are co-expressed in the future cartilaginous elements. Sox9 expression in the ceratohyal is also diminished by stage 41 with the onset of chondrogenesis. Col2a1 is distributed through the notochord and otic capsule along with a subset of the branchial arches (BA) and presumptive suprarostral plate by stage 33/34. Col2a1 is expressed widely throughout the head during the stages examined with intensifying staining in the presumptive cranial cartilages by stages 39 and 41. The runx cofactor cbfb is expressed throughout the head during development, with stronger expression in the presumptive ceratohyal and palatoquadrate by stage 39.

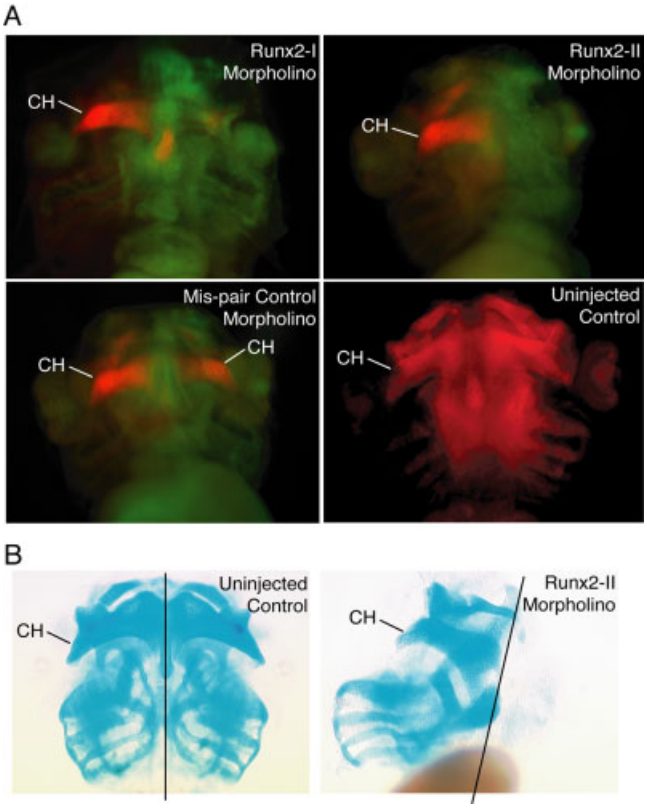

Fig. 4.

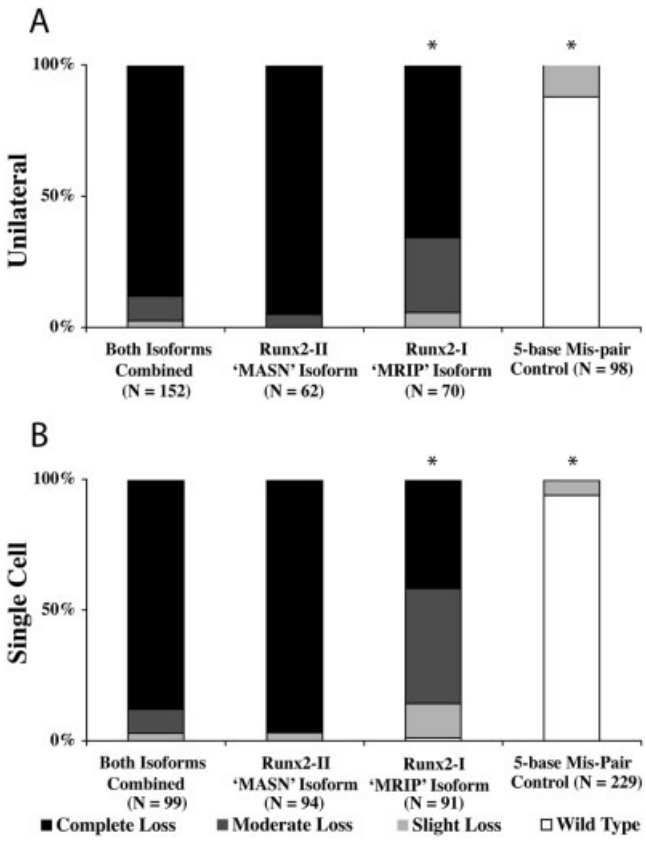

Fig. 5.

Fig. 4. Effects of morpholino antisense oligonucleotide injections on cartilage formation. All images are ventral views of larval skulls with anterior at the top. **A:** Cartilages stained with anti-collagen II antibody appear red. Morpholino-injected cell lineages appear green. The effects of both runx2 isoform-specific morpholinos are shown along with a mis-pair control morpholino and an uninjected control. Cartilage formation is prevented on the injected side of both anti-runx2 morpholinos, but is normal in the mis-pair control and uninjected control. **B:** Cartilage formation defect due to an anti-runx2-II morpholino revealed through Alcian blue staining in a stage-46 tadpole. Black line marks the midline of each embryo. CH, ceratohyal cartilage.

Fig. 5. Anti-runx2 morpholino effects on cartilage formation. Cartilage loss in combined isoform-specific morpholinos are compared to individual isoform-specific morpholinos and the 5-base mis-pair control. **A:** Effect of unilateral injection into a two-celled embryo on subsequent cartilage formation. Failure to form cartilage was always confined to the injected side. **B:** Effect of injection into a single-celled zygote on later cartilage formation. Failure to form cartilage was observed on both sides. A,B: Each anti-runx2 morpholino treatment was significantly different from the mis-pair controls from both unilateral and single-cell injections ($P < 0.0001$ asterisks above "5-base mis-pair control"). The runx2-II and "Both Isoform" morpholino treatments also significantly differed from the runx2-I isoform in from both unilateral ($P < 0.0015$) and single-cell ($P < 0.0001$) injections (asterisks above runx2-I). There was no significant difference between the runx2-II and "Both Isoform" treatments from either unilateral ($P = 0.4025$) or single-cell ($P = 0.1136$) injections.

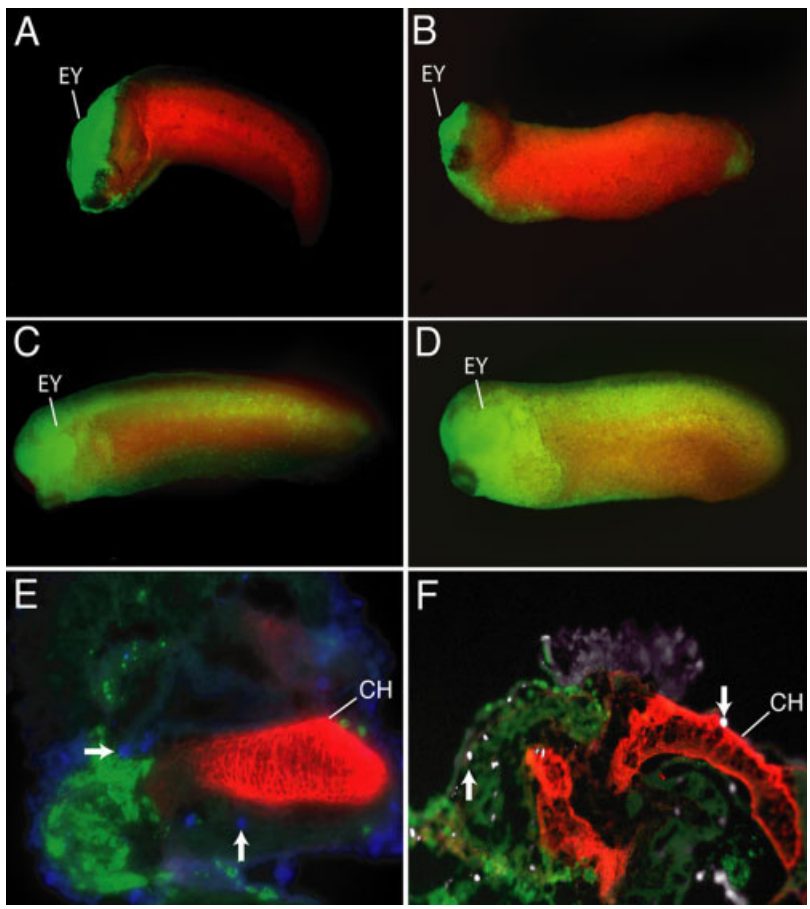

Fig. 6.

over the next several developmental stages. By stage 39, expression of sox9 is mostly restricted to the same areas that express runx2; corresponding to condensations of the suprarostral plate (Fig. 2A), palatoquadrate, ceratohyal, and ceratobranchials (Figs. 2B, 3). The mRNA of both genes is distributed in a loop that runs along the mandibular arch and connects to the cranial trabeculae and suprarostral plate anlagen dorsally (Fig. 2B). This loop corresponds to different regions of the palatoquadrate cartilage. The posterior-most segment of the loop is the future subocular arch. The anterior-most segment is the future quadratocranial commissure, which connects the palatoquadrate with the anterior neurocranium. Medial to these loops are faint processes of skeletal anlagen that correspond to the future infrarostral and Meckel's cartilages. These small processes enlarge and join at the midline by stage 41 (Fig. 2A). Sox9 staining at stage 41 reveals a continuous band of skeletal precursors between the paired Meckel's cartilages and the fused infrarostrals. Separation of the medial infrarostals from the lateral Meckel's cartilages occurs later in development and may coincide with the activity of skeletal segmentation-specific genes (Newman and Krieg, 1999; Svensson and Haas, 2005).

Expression of both runx2 and sox9 decreases in the ceratohyal by stage 41 as this cartilage begins to chondrify (Fig. 3). Both genes are eventually undetectable in more mature cartilages (data not shown). Runx2 staining also is present for the first time in the otic capsule, which does not begin to form cartilage matrix until stage 46 (Nieuwkoop and Faber, 1994). The early expression of sox9 in the otic capsule is also diminished as the capsule begins to chondrify.

The cartilage-dominant collagen, col2a1, is restricted to the otic capsule and notochord along with a subset of the branchial arches and future suprarostral plate at stage 33/34. Its expression co-localizes with runx2 and sox9 in the precursors of the palatoquadrate and ceratohyal by stage 39, and by stage 41 it is also found in the ceratobranchial anlagen. Epithelial staining also increases during these later stages (Fig. 3).

The runx co-factor cbfb is essential for proper runx2 function in the amniote skeleton (Kundu et al., 2002). In *Xenopus*, cbfb mRNA is widely distributed throughout the head during embryonic development. By stage 39, its expression intensifies in the palatoquadrate and ceratohyal anlagen, possibly indicating the onset of runx2 function in these cartilaginous precursors (Fig. 3).

Effects of Anti-Runx2 Morpholinos on Cartilage Formation

Morpholinos targeting the 5′ UTR of both runx2 isoforms were injected into two-celled embryos and single-celled zygotes. Distribution of each morpholino was tracked with a fixable fluorescent dextran, which was co-injected as a lineage tracer. Cartilage loss is evident in both cleared-and-stained and anti-collagen-II antibody-stained preparations (Figs. 4, 5). Cartilage loss was scored through analysis of the hyobranchial skeleton, although more extreme loss included absence of the cartilaginous neurocranium as well (Fig. 4B). The runx2-II specific morpholino causes cartilage loss on the injected side in 100% of unilaterally injected embryos, with complete loss on the injected side in 95% (N = 62). The runx2-I specific morpholino also causes a cartilage loss in 100% of unilateral injections, with 65% showing complete cartilage loss on the injected side (N = 71). A mis-pair morpholino, which shares all but five bases with the runx2-I isoform, was used as a control. This morpholino causes only slight loss of the ceratobranchials in 12% of the injected embryos, whereas 88% are wild type (N = 99). The runx2-II and runx2-I morpholinos combined cause cartilage loss in 100% of unilaterally injected embryos; 89% show complete loss on the affected side (N = 151). Results from single-celled zygote injections are similar to the two-celled embryo injections. The runx2-II morpholino causes cartilage loss in 100% of injected embryos, with 97% showing complete loss (N = 94); the runx2-I morpholino causes cartilage loss in 99% of injected embryos, with 42% exhibiting complete loss (N = 91); and the two morpholinos combined causes cartilage loss in 100% of injected embryos, with 88% showing complete bilateral loss (N = 99). The 5-base mispair control causes a slight loss on the injected side in 6% of embryos, with 94% showing a wild-type phenotype (N = 229). This slight loss may be attributable to partial binding of the control morpholino to the target sequence.

There is a highly significant difference between the cartilage loss observed in the anti-runx2 morpholino-injected groups compared to the 5-base mis-pair control from both unilateral and single-cell injections (Pearson's chi-square tests; df = 3, $P < 0.0001$; Fig. 5). This difference is more pronounced in the runx2-II and

Fig. 6. Anti-runx2 morpholinos knock down EGFP protein production (A–D), and the combined morpholinos have no apparent effect on cell death or cell proliferation (E,F). A–D: Combined fluorescent images of stage-33/34 embryos; lateral views; anterior to the left. A portion of the right side is visible in A and B due to body torsion. The green cells are expressing egfp, and the red cells are the morpholino-injected lineage revealed through a rhodamine dextran lineage tracer. **A:** Unilateral knockdown of egfp protein production following an initial injection of the zygote with pCS2:runx2-I 5′:egfp mRNA, and a second injection with the anti-runx2-I morpholino (red) after the first cell division. **B:** Same experiment as A with the runx2-II isoform sequence attached to the egfp (green), and anti-runx2-II morpholino (red) injected after the first cell division. Both isoforms are capable of inhibiting egfp production in one half of the embryo, resulting in no overlay of the egfp and rhodamine dextran. **C,D:** The reciprocal morpholino injections do not inhibit egfp production. Unilateral injection of the runx2-II morpholino did not inhibit pCS2:runx2-I 5′:egfp mRNA (C), and the unilateral injection of the runx2-I morpholino did not inhibit pCS2:runx2-II 5′:egfp mRNA expression (D). **E,F:** Coronal sections of stage-42 hatchlings injected with combined anti runx2 morpholinos; anterior is to the top. Both are overlaid fluorescent images of rhodamine, FITC, and cy5 channels. Morpholinos were injected in a two-cell embryo along with the fluorescein dextran (green). The hatchling is stained with both anti-collagen-II (red) and either anti-caspase-3 to assay apoptosis (blue in E), or anti-phospho-histone-3 to assay mitosis (white in F). Both apoptosis and cell proliferation are evident on the morpholino-injected and uninjected sides (white arrows in both E and F), and neither marker is overexpressed in the morpholino-injected mesenchyme that has failed to form cartilage. EY, eye; other abbreviations as in Figure 4.

"Both Isoform" groups than the runx2-I group, which has a less consistent cartilage-loss phenotype (Fig. 5). There are significant differences between the effects of the runx2-I and runx2-II morpholinos (Pearson's chi-square; unilateral X = 17.8, df = 3, $P = 0.0005$, bilateral X = 66.6, df = 3, $P < 0.0001$), and between the runx2-I morpholino and both isoform-specific morpholinos combined (unilateral X = 16.0, df = 3, $P = 0.0012$, bilateral X = 45.0, df = 3, $P < 0.0001$). However, the slight differences between the runx2-II morpholino and both isoform-specific morpholinos combined were insignificant (unilateral X = 2.9, df = 3, $P = 0.4025$, bilateral X = 6.0, df = 3, $P = 0.1136$).

Morpholino Controls

Several morpholino controls were performed. These included knocking down egfp translation with the anti-runx2 morpholinos, testing mitotic activity and apoptosis in the morpholino-injected cells, and rescuing the morpholino injections with full-length runx2 mRNA injections. Unilateral egfp knockdowns were performed to test the anti-runx2 morpholinos' ability to inhibit translation. This required two sequential injections into the same embryos. The 5′ runx2-II and runx2-I isoform sequences were inserted just before the translation start site on a pCS2:egfp construct. Synthetic egfp mRNA was then injected into single-celled zygotes. After the first cell division, runx2-II or runx2-I morpholinos were injected into one blastomere of the two-celled embryo along with a rhodamine dextran lineage tracer. The resulting stage 33/34 embryos showed unilateral expression of the EGFP protein as determined by fluorescence microscopy (Fig. 6A,B). The dextran label was distributed on the side that did not express EGFP protein, indicating that the morpholinos are capable of preventing protein translation. The reciprocal experiment was also performed; egfp constructs were injected in the zygote and the non-corresponding morpholino was injected into the two-celled embryo. The resulting embryos co-express both EGFP and carry the rhodamine lineage tracer on the morpholino-injected side (Fig. 6C,D).

Two polyclonal antibodies were used to investigate the condition of morpholino-injected cells. An anti-caspase-3 antibody was used to detect apoptosis in morpholino-injected hatchlings. Caspase-3-positive cells were evenly distributed on injected and unjected sides, indicating that the anti-runx2 morpholino did not increase apoptosis in the pre-cartilaginous mesenchyme (Fig. 6E). An anti-phospho-histone-3 antibody was used as a mitosis marker to determine whether morpholino toxicity was responsible for cartilage loss. Histone-3 was evenly expressed between injected and uninjected sides of the stage 42 tadpole, indicating that morpholino injection did not affect normal cell division.

Single-cell morpholino injections of both transcripts were rescued with exogenous full-length runx2 mRNA (Fig. 7). Morpholinos were co-injected with fluorescein-labeled dextran into the single-celled zygote, and full-length isoform-specific mRNA's were co-injected with rhodamine-labeled dextran after the first cell division. Cartilages stained with the collagen II antibody were found in stage 42 hatchlings on the mRNA-injected sides (Fig. 7).

Neural Crest Transplants Reveal the Timing of Runx2 Function

Reciprocal cranial neural crest transplants were performed between wild type and morpholino-injected embryos. In both sets of experiments, ectoderm of the neural fold was peeled back on the right side of a host embryo and a portion of the underlying cranial neural crest was removed. These cells then were replaced by a corresponding portion of neural crest from the same region of a donor embryo. In one experiment, a section of neural crest was transplanted into a wild-type host from donors injected in one of two cells with the combined runx2-I and runx2-II morpholinos plus fluorescein dextran. After 24 hr, the transplanted neural crest was observed migrating ventrally from the neural tube along the visceral arches. Portions of the hyoid and branchial migratory streams contained dextran-positive donor cells (Fig. 8A). By stage 44, these hosts exhibited a reduction in the ceratobranchial cartilage, a hyoid arch crest derivative, in a distal region populated by the morpholino-injected cells (Fig. 8B). The reciprocal experiment was also performed, in which wild-type crest was transplanted into a morpholino-injected embryo (Fig. 8C,D). The wild-type donor was labeled with rhodamine dextran, and the transplanted neural crest was observed migrating in the hyoid stream at stage 33/34 (Fig. 8C). While the dextran label did not persist through the antibody staining, a partial rescue of the ceratobranchial was observed on the transplanted side (Fig. 8D).

Migration of neural crest cells in morpholino-injected specimens was also characterized with sox9 in situ hybridization. Distribution of this transcript is identical on both sides of an individual injected with the combined runx2 morpholinos in a two-celled embryo, with strong expression in the migrating neural crest, otic capsule, eye, and brain (Fig. 8E,F). Overexpression of either runx2 isoform through single-cell mRNA injection also failed to affect the distribution of sox9 transcripts (data not shown).

DISCUSSION

This study reveals an important role of the transcription factor Runx2 in larval cartilage differentiation in the frog, *Xenopus laevis*. Runx2 mRNA is initially expressed in a subset of sox9-expressing cranial neural crest cells in the embryo. In subsequent stages, both transcription factors are co-expressed in cartilage precursors. Their distributions correspond to some of the earliest patterning of the larval head skeleton. The role for Runx2 in the formation of the larval hyobranchial skeleton was investigated through anti-runx2 morpholino oligonucleotides. Neural crest transplants between morpholino-injected and wild type embryos reveal a normal pattern of crest migration in runx2-deficient cells, which fail to form chondrocytes detectable through the collagen-II antibody. This indicates a role for runx2 in the terminal differentiation of the crest-derived chondrocyte lineage. While several morpholino-injected individuals also exhibit loss of mesoder-

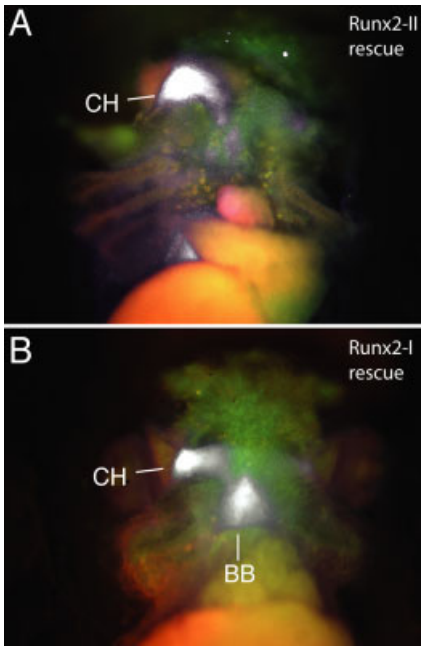

Fig. 7. Morpholino injections rescued with full-length runx2 messenger RNA injections. An anti-runx2 morpholino was co-injected into a single-celled zygote with fluorescein dextran (green) and the corresponding full-length runx2 mRNA was co-injected with rhodamine dextran after the first cell division. A,B: Ventral views of the chondrocranium stained with the anti-collagen-II antibody (white). **A:** The unilateral runx2-II mRNA partially rescues the ceratohyal (CH) on the injected side. **B:** The unilateral runx2-I mRNA partially rescues the ceratohyal and basibranchial (BB) on the injected side. The rhodamine label faded during the antibody staining.

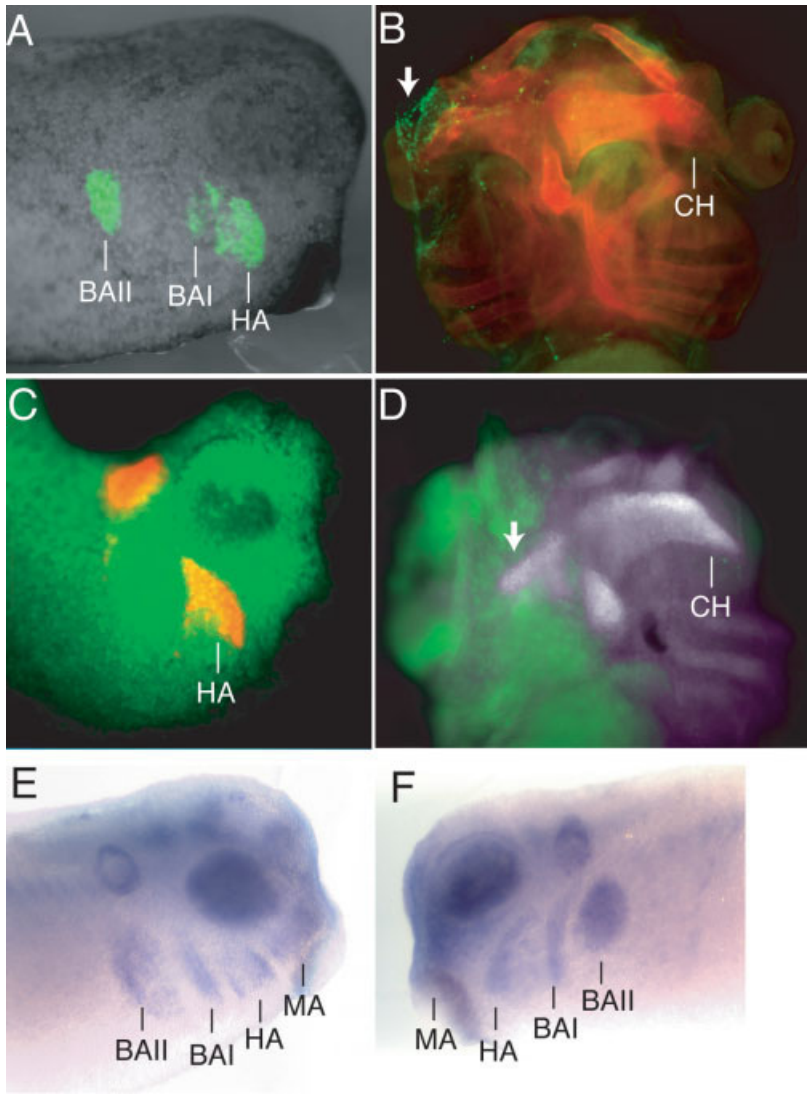

Fig. 8. Anti-runx2 morpholino injections do not affect cranial neural crest cell migration. A and C are lateral views of live stage-33/34 hosts that have received neural crest transplants. B and D are the stage-44 hatchlings of the same individuals as A and C, which have been stained with the anti-collagen II antibody (red in B, white in D). **A:** Live image of a wild-type host that has received neural crest from a morpholino-injected donor. Portions of the presumptive hyoid and branchial neural crest streams have been replaced with morpholino-injected cells (green), which are migrating normally. **B:** Same individual as A at stage 44, stained with anti-collagen II to reveal cartilage formation (red). The ceratohyal cartilage is truncated on the transplanted side, with a population of donor cells derived from the hyoid stream concentrated on the distal end (arrow). C,D: Neural crest transplanted from a wild-type donor into a morpholino-injected host can rescue cartilage loss. **C:** Live image of a morpholino-injected host that has received wild-type neural crest. The rhodamine labeled wild-type crest (red) migrates normally in the morpholino-injected host (green). **D:** Same individual as C at stage 44, stained with anti-collagen II (white). The ceratohyal is partially rescued on the morpholino-injected side (arrow). The rhodamine-label of the wild-type crest did not persist through antibody staining. E,F: Sox9 in situ hybridization in a single stage-32 embryo unilaterally injected with both runx2-I and runx2-II isoform-specific morpholinos. **E:** Wild-type side of the embryo, showing normal neural crest morphology revealed by the distribution of the sox9 probe. **F:** Anti-runx2-morpholino-injected side showing the same sox9 staining pattern as the wild-type side. The fluorescein label did not persist through the whole mount in situ hybridization. Abbreviations as in Figures 2 and 4.

mally derived cartilages in the neurocranium (Fig. 4B), only hyobranchial skeletal loss was screened due to its early formation in *Xenopus* embryos.

Early Cranial Patterning Revealed by Runx2 and Sox9 Distribution

Co-expression of runx2 and sox9 mRNA in precursors of the larval skull reveals the earliest pre-patterning of the tadpole chondrocranium yet reported. Extensive expression of sox9 in the neural crest overlaps the more limited expression of runx2 in the mesenchymal precursors of Meckel's cartilage, the palatoquadrate, and the suprarostral plate (Fig. 2A). By stage 39, both transcription factors are mostly co-expressed in a pattern that closely corresponds to the future skeletal elements (Fig. 2B). The anlagen for these cartilages do not appear as distinct condensations until stage 40 (Sadaghiani and Thièbaud, 1987; Seufert et al., 1994) and do not form cartilage matrix until stage 42 (Nieuwkoop and Faber, 1994).

The unique expression pattern of runx2 may resolve a long-standing debate regarding the homology of the suprarostral plate, a unique cranial cartilage found in *Xenopus* and other members of the family Pipidae. Most

anurans have paired suprarostral cartilages that constitute the larval upper jaws. These cartilages form initially as separate chondrogenic condensations in the anterior ethmoid region, which later fuse with the cranial trabeculae posteriorly (e.g., *Rana temporaria*; Spemann, 1898; reviewed in de Beer, 1937). Paired suprarostral condensations are not seen in standard histological reconstructions of early *Xenopus* embryos (Föske, 1934; reviewed in Roček, 2003). Instead, a single, continuous and median plate of cartilage is first visible in histological sections through the anterior ethmoid region. Several studies have accepted the homology between the paired suprarostrals of most anurans and the median suprarostral plate of pipids (Sokol, 1975, 1977; Trueb and Hanken, 1992; Swart and de Sá, 1999; Pugener et al., 2003). Others, however, have denied this homology because the suprarostral plate does not appear to form from paired chondrogenic precursors (de Beer, 1937; Sedra and Michael, 1957; Roček and Vesley, 1989; Roček, 2003). Some even have accepted an alternative name for the median cartilage as the ethmoid trabecular plate (Sadaghiani and Thièbaud, 1987; Nieuwkoop and Faber, 1994). Both runx2 and sox9 are expressed in the precursors of the suprarostral plate in *X. laevis* as early as stage 31, several stages before overt cartilage differentiation is detected by standard histological techniques. The expression of runx2 shows, for the first time, that the larval suprarostral plate does arise from paired anterior anlagen (Fig. 2A). These precursors fuse in the midline by stage 41, creating a plate of continuous staining before the condensation fully differentiates as cartilage. This result provides strong support for the homology between the paired suprarostral cartilages of most larval anurans and the suprarostral plate of *Xenopus* and other pipid frogs.

The ventral portion of the mandibular crest stream gives rise to the larval lower jaw (fused infrarostrals and Meckel's cartilage) and its suspension (palatoquadrate) (Sadaghiani and Thièbaud, 1987). The distribution of runx2 and sox9 mRNA in the ventral mandibular crest reveals the early patterning of these cartilages. The palatoquadrate initially appears as a ventrally directed loop of staining. By stage 39, the anterior arm of this loop is continuous with the dorsal and anterior cranial trabeculae along with the precursors of the suprarostral plate (Fig. 2B). This portion of the palatoquadrate corresponds to the future quadratocranial commissure. The posterior section of the loop corresponds to the future subocular arch of the palatoquadrate. This arch eventually fuses to the ventrolateral process of the neurocranium, which forms the larval ascending and otic processes (Trueb and Hanken, 1992). The medial and ventral portion of the loop is continuous with a faint patch of staining, which corresponds to the future Meckel's and infrarostral cartilages. This early distribution reveals a lateral to medial formation of the palatoquadrate, Meckel's, and fused infrarostral cartilages within the mandibular arch.

Runx2 mRNA is not expressed in the presumptive cartilaginous otic capsule until stage 41, well after the expression of both sox9 and col2a1 in this cartilage. This later staining of runx2 corresponds to the initial formation of the otic capsular cartilages, which appear at stage 46 (Nieuwkoop and Faber, 1994). The otic capsules and posterior cranial trabeculae provide the only two examples of runx2 expression in non-crest-derived cartilages (Sadaghiani and Thièbaud, 1987). The relatively late formation of these cartilages makes assessment of runx2 function in their differentiation difficult. Several stage-46 cleared-and-stained tadpoles injected with both morpholinos lack cranial trabeculae and otic capsules (Fig. 4B), as has been demonstrated for zebrafish runx2b-II (Flores et al., 2006). However, many hatchlings recover from the effect of morpholinos by this stage. While the translation of runx2 can be inhibited through morpholino oligonucleotides during hyobranchial cartilage formation, other methods of gene silencing are required to sufficiently determine its function in the rest of the larval chondrocranium, and in the differentiation of cartilage and bone during metamorphosis.

Isoform-Specific Differences

We were able to inhibit the translation of individual runx2 isoforms by injecting morpholinos that target the 5′ untranslated region and first exon of either runx2-I or runx2-II. Silencing *Xenopus* runx2-II creates a significantly stronger and more consistent cartilage loss phenotype (Fig. 5). This stronger effect is shared with the zebrafish runx2b-II morpholino in comparison with runx2b-I (Flores et al., 2006). Mouse cell culture studies also have found the RUNX2-II protein to have a greater effect on regulating the osteocalcin gene than RUNX2-I (Harada et al., 1999), which indicates a stronger role for this isoform as a transcription factor during bone formation. The stronger effect of the runx2-II isoform over runx2-I appears to be conserved in the formation of both bone and cartilage. The combined injection of both isoform-specific morpholinos created an effect that was intermediate between the runx2-II and runx2-I morpholinos. This combined-morpholino effect was still statistically different from the runx2-I morpholino effect, and not statistically different from the runx2-II morpholino (Fig. 5).

The Evolution of Cartilage Differentiation

Studies in mouse and chicken have shown *Runx2* mRNA to be transcriptionally active in the early cartilaginous skeleton (Inada et al., 1999; Enomoto et al., 2000, 2004; Enomoto-Iwamoto et al., 2001; Iwamoto et al., 2003; Eames et al., 2004). However, neither species requires the gene product to be functional during early cartilage formation. Runx2′s inactivity during amniote cartilage formation may be attributed to several different levels of regulation imposed on the gene product (Franceschi and Xiao, 2003; Xiao et al., 2003; Wang et al., 2004; Bae and Lee, 2005; Lengner et al., 2005; Goldring et al., 2006). A change in post-transcriptional modification of Runx2 or in the function of one of its co-factors may account for the possible evolutionary loss of the transcript's function during cartilage formation within the amniote lineage. There is some evidence that the RUNX1 protein has an earlier functional role in mouse limb cartilage formation, which may replace any functional requirements for the RUNX2

protein in these cartilages (Smith et al., 2005; Wang et al., 2005). Additionally, runx1 morpholinos have no effect on early zebrafish cartilage formation (Flores et al., 2006). The function of Runx1 and Runx3 proteins in cartilage formation has not been investigated in *Xenopus*. Such additional studies would help resolve the evolution of runx gene function in vertebrate skeletal development.

The developmental role of runx2 in *Xenopus* and zebrafish larval cartilage differentiation is shared with amniote secondary cartilage formation. *Runx2* knockout mice do not form the condylar cartilage, which suggests a role for RUNX2 protein in its differentiation (Shibata et al., 2004, 2006). This cartilage may be derived either from the periosteum of the dentary or from a sesamoid that is independent from the rest of the developing jaw (reviewed in Hall, 2005, p 155–159). The missing condyle shows an interesting parallel to cartilage loss in *Xenopus* and zebrafish injected with anti-runx2 morpholinos. These similarities may indicate a shared mode of differentiation between certain types of cartilages and at the same time reveal an unexpected developmental diversity in vertebrate skeletogenesis.

EXPERIMENTAL PROCEDURES

Cloning of *Xenopus laevis* runx2

Xenopus laevis runx2 was amplified from bone-derived cDNA using degenerate PCR. The initial fragment amplified was a 528–base pair (bp) product. The 5′ and 3′ regions of the gene were subsequently amplified from the pDNR:Tad2 cDNA library (a gift from Dr. Donald Brown) through PCR. Internal forward and reverse primers were designed from the initial *Xenopus laevis* runx2 sequence and used along with the M13 sequencing primers in the library's pDNR vector. Two separate isoforms were amplified and cloned into the pCRII vector using the Invitrogen "TOPO TA" cloning kit. A 1.2-Kb fragment was also cloned into the pCRII vector and used to synthesize antisense RNA probe for in situ hybridizations. Specific forward primers were designed for both the runx2-II and runx2-I isoforms and used to amplify full-length transcripts from *Xenopus laevis* bone-derived cDNA with a 3′ UTR reverse primer based on the *Xenopus tropicalis* genomic sequence. These 1,831-bp (runx2-II; Genbank accession EF029871) and 1,856-bp (runx2-I; EF029872) products were sub-cloned into the EcoR1 sites of the pCS2 expression vector for in vitro transcription and mRNA injections.

Runx2 Alignments

Mouse *Runx2* (GenBank accession; Q08775), and *Danio rerio runx2a* (47086321) and *runx2b* (47086313) were downloaded in FASTA format and edited using Mesquite (Maddison and Maddison, 2005). Protein sequences were aligned in ClustalX (Chenna et al., 2003). The *Xenopus laevis* cDNA sequence was pair-wise blasted against scaffold 328 of the *Xenopus tropicalis* draft genome sequence (Joint Genome Institute, Walnut Creek, CA) to determine intron-exon structure.

RT-PCR Analysis of Runx2 Isoforms

Whole-embryo and tissue-specific cDNAs were synthesized from total RNA. Animals were euthanized with buffered tricaine methane sulfonate (MS-222; pH 7.4). cDNA was synthesized for Nieuwkoop and Faber (1994) stages 7, 20, 25, 33/34, 42, 59, and 62, and for adult long bone (humerus) and stage-59 tadpole brain. One microgram of total RNA was used for each reverse-transcription reaction. Specific forward primers for both isoforms were used along with a conserved internal reverse primer to give 457-bp (runx2-II) and 415-bp (runx2-I) products. A 250-bp region of the *Xenopus laevis* histone-4 gene was amplified from these tissues as a positive control (Ding et al., 1998). Single replicates of each PCR were performed to verify the results.

In Situ Hybridizations

Probes for in situ hybridization were generated with digoxygenin-conjugated UTP (Roche, Indianapolis, IN) using Ambion (Austin, TX) "Maxiscript" transcription kits. Anti-runx2 riboprobe was generated from a 1.2-Kb region of *Xenopus laevis* runx2 that is shared by both isoforms. Antisense probes also were generated for *Xenopus laevis* pGEMT:sox9 following the protocol of Spokony et al. (2002), and for pCS2-AS-collagen II following the protocol of Larrain et al. (2000). An anti-cbfb probe was generated from an EST clone (XL065o21) provided by Dr. Naoto Ueno of the National Institute of Basic Biology (Okazaki, Japan).

Whole-mount in situ hybridizations were performed on albino embryos following Sive et al. (2000). Embryos were fixed in MEMFA and stored in 70% ethanol at −20°C prior to initial use. All hybridizations were carried out overnight at 55°C. Stained embryos were stored in 70% glycerol at 4°C.

Morpholino Antisense Oligonucleotide and mRNA Injections

Antisense morpholino oligonucleotides were targeted to the 5′ untranslated regions (UTRs) of the two *Xenopus laevis* runx2 isoforms. Isoform-specific morpholino sequences were 5′ TACGGGAATACGCATCACAACAGCC 3′and 5′ TGTTGGACGCCATTGACTTTCTTGC 3′ for runx2-I and runx2-II, respectively. A control morpholino was also used, which differed from the runx2-I sequence by five base pairs (5′ TACGGCAATAGCCATCAGAACACCC 3′; mis-paired bases underlined). All morpholinos were supplied by GeneTools (Philomath, OR).

Gametes were harvested and fertilized, and the resulting zygotes dejellied following the protocols of Sive et al. (2000). Between 50 and 60 ng of morpholino were injected, in a volume of 10 nl, into either single-celled zygotes or two-celled embryos with a Femtojet microinjector (Eppendorf, NY). This concentration and the injection procedures followed the protocol of Khokha et al. (2005). Combined isoform knockdowns were performed by mixing and co-injecting 25 ng of each morpholino. A fluorescein-labeled dextran (6.25 mg/ml, lysine fixable, Invitrogen) was co-injected as a lineage tracer of morpholino-injected cells. Injections were carried out in 0.5× MMR with 4% Ficoll (EM Science,

Darmstadt, Germany). Injected embryos were immediately transferred to 0.3× MMR with 4% Ficoll. After 24 hr, the embryos were transferred into 0.1× MMR without Ficoll. Embryo culture solutions were supplemented with 50 μg/ml gentamycin to prevent infection. Embryos were raised in the dark at 18°C for six days before the cartilage-loss phenotype was scored.

Full-length runx2 mRNA injections were performed to rescue the cartilage-loss phenotype. The pCS2:MASNrunx2 and pCS2:MRIPVrunx2 vectors were linearized with Not1 and transcribed with the SP6 RNA polymerase using a "mMessage mMachine" kit (Ambion). Between 50 and 60 ng of morpholino was injected into the single-celled zygotes with fluorescein-labeled dextran. A total of 600 pg of mRNA was injected into one side of the same embryos after their first cell division, along with a rhodamine-labeled dextran (6.25 mg/ml, lysine fixable, Invitrogen). Embryos were raised to stage 42 and scored for cartilage gain on the mRNA-injected side.

Phenotype Scoring and Immunohistochemistry

Cartilage-loss phenotypes of morpholino-injected hatchlings were assayed using an anti-collagen II monoclonal antibody (1:100, Linsenmayer and Hendrix, 1980) in conjunction with the dextran lineage tracer. This antibody has been effective as a marker for early stages of cartilage formation in *Xenopus laevis* (Seufert et al., 1994). Several specimens were also stained with an anti-phospho-histone-3 polyclonal mitosis marker (1:500; Upstate Biotechnology, Lake Placid, NY) to assess the survival of the injected cell lineage, or the anti-caspase-3 apoptosis marker (1:500; BD-Biosciences, Franklin Lakes, NJ) to assess apoptosis in the morpholino-injected cells (after Schreiber et al., 2001). Hatchlings were fixed in 4% PFA and stored in PBS prior to immunohistochemistry. Following permeabilization with 10 μg/ml of proteinase K and refixation in 4% PFA, specimens were dehydrated in methanol and bleached in Mayor solution (Mayor et al., 1995). Specimens were blocked in PBS containing 5% normal goat serum (Gemini Bio-Products, Woodland, CA) and incubated in primary antibodies overnight at 4°C. After several washes in PBST, a goat-anti-mouse Alexa Fluor 546 secondary antibody (Invitrogen) was added for monoclonal antibodies, and a goat-anti-rabbit Alexa Fluor 647 (Invitrogen) was added for polyclonal antibodies. Goat-anti-mouse Alexa Fluor 647 was used for the wild-type neural crest transplants and mRNA rescue experiments. Embryos were again incubated overnight at 4°C, washed and photographed in 75% glycerol. Double-stained collagenII/phospho-histone-3 and collagenII/caspase-3 specimens were embedded in OCT, frozen, and sectioned at 10 μm after whole-mount staining.

The cartilage-loss phenotype was scored according to the amount of individual element loss from the hyobranchial skeleton. This loss varied in severity from the lateral to medial ends of each paired cartilage, and from posterior to anterior within the hyobranchial skeleton. Less severe effects only truncated lateral ends of the ceratobranchial cartilages, whereas more severe effects also truncated the lateral ends of the larger ceratohyal cartilage. This latter element was lost entirely in the most dramatically affected hatchlings, along with the ceratobranchials. The most dramatically affected embryos also consistently failed to form the neurocranium on the injected side. Scoring of the cartilage loss phenotype followed this pattern of effect. Absence of cartilage in dextran-positive regions of the chondrocranium was designated "complete loss"; loss of the ceratobranchials and most of the ceratohyal was designated "moderate loss"; reduction of the ceratobranchials with a normal ceratohyal was designated "slight loss"; and retention of the entire cartilaginous skeleton was designated "wild type." Embryos injected with morpholinos in one-celled zygotes were compared to uninjected controls from the same clutch. Embryos injected after the first cell division exhibited a unilateral distribution of the dextran lineage tracer, and cartilage was affected on only one half of the hatchling. These were also compared with wild type hatchlings from the same clutch along with the unilaterally unaffected side of the same experimental animal.

Cartilage Staining

Specimens were cleared and stained according to the protocol of Dingerkus and Uhler (1977) with the exclusion of alizarin red steps, which are used to stain bone. Samples were fixed in 10% neutral-buffered formalin (Sigma), dehydrated in ethanol, and stained for several hours in an 8GX Alcian blue working solution. Samples were then rehydrated and macerated in 1% trypsin in 30% saturated aqueous sodium borate. They were transferred to 100% glycerol for clearing and photography.

EGFP Translation Inhibition Controls

Isoform-specific morpholino sequences were inserted into the 5′ region of a pCS2:egfp construct. Complimentary oligonucleotides matching the target sequence of the morpholinos were designed with 5′ BamH1 and 3′ Nco1 overhangs. The oligonucleotides were combined in an annealing buffer of 40 mM Tris, 20 mM $MgCl_2$, and 50 mM NaCl, heated to 100°C for 5 min, and allowed to cool to room temperature. Constructs were ligated into BamH1/Nco1 double-cut pCS2:egfp. The final construct was then linearized and transcribed with SP6 (mMessage mMachine; Ambion). Single-celled *Xenopus laevis* zygotes were injected with 1,000 pg of the morpholino-sequence-linked egfp mRNA. After the first cell division, the same embryos were injected again with the isoform-specific morpholino using the protocol described above. A rhodamine-labeled dextran lineage tracer (6.25 mg/ml, Invitrogen) was co-injected with the morpholinos instead of the fluorescein-labeled dextran to contrast the EGFP protein expression. The reciprocal experiment was also performed, where the injected isoform-specific morpholino did not correspond to the egfp construct sequence.

Neural Crest Transplants

Grafts of embryonic cranial neural crest were transplanted between neurula stage wild-type and morpholino-injected embryos following the protocol of Gross and Hanken (2004). Briefly, a piece of overlying ectoderm was cut on three sides to access the underlying neural crest on the right

side of the neural plate. The crest cells were removed in host embryos and replaced with cells from the same location in stage-matched donors. One experiment consisted of transplanting combined runx2-II and runx2-I morpholino-injected cells, labeled with the fluorescein dextran, into a wild-type host. An additional experiment consisted of transplanting wild-type neural crest, labeled with rhodamine dextran, into a host injected with both anti-runx2 morpholinos. Morpholinos were injected into one cell of two-celled embryos following the protocol described above. These embryos were later screened for a unilateral distribution of dextran before transplantation. In both sets of transplants, a large portion of the presumptive hyoid stream was transferred along with smaller portions of the branchial streams. The hyoid stream-derived ceratohyal cartilage showed the most dramatic loss or gain in each of the two experiments (Fig. 8A–D). Embryos were raised at room temperature to stage 44. They were then stained with the collagen II antibody to reveal cartilage gain or loss in the transplanted cells.

ACKNOWLEDGMENTS

The authors thank the generous donors of *Xenopus laevis* probes: Jean-Pierre Saint-Jeannet (sox9), Naoto Ueno (cbfb), and Edward DeRobertis (col2a1). Bjorn Olsen and members of his laboratory, especially W. Wang, N. Fukai, and E. Zelzer, were extremely helpful in the cloning of *Xenopus* runx2 and for their advice over several years. Thanks to D. Blackburn and W. Wang for commenting on an earlier version of this manuscript. Funding was provided by NSF Amphibia Tree (EF-0334846; J.H.), NIH Genetics and Genomics Training Grant (R.K.), and Sigma-Xi Grant in Aid of Research (R.K.).

REFERENCES

Bae SC, Lee YH. 2005. Phosphorylation, acetylation and ubiquitination: The molecular basis of RUNX regulation. Gene 366:58–66.

Banerjee C, McCabe LR, Choi JY, Hiebert SW, Stein JL, Stein GS, Lian JB. 1997. Runt homology domain proteins in osteoblast differentiation: AML3/CBFA1 is a major component of a bone-specific complex. J Cell Biochem 66:1–8.

Blyth K, Cameron ER, Neil JC. 2005. The RUNX genes: gain or loss of function in cancer. Nat Rev Cancer 5:376–387.

Cameron ER, Blyth K, Hanlon L, Kilbey A, Mackay N, Stewart M, Terry A, Vaillant F, Wotton S, Neil JC. 2003. The Runx genes as dominant oncogenes. Blood Cells Mol Dis 30:194–200.

Chenna R, Sugawara H, Koike T, Lopez R, Gibson T, Higging D, Thompson J. 2003. Multiple sequence alignment with the Clustal series of programs. Nucleic Acid Res 31:3497–3500.

Choi KY, Lee SW, Park MH, Bae YC, Shin HI, Nam S, Kim YJ, Kim HJ, Ryoo HM. 2002. Spatio-temporal expression patterns of Runx2 isoforms in early skeletogenesis. Exp Mol Med 34:426–433.

de Beer G. 1937. The development of the vertebrate skull. Oxford: Clarendon Press.

Ding X, Hausen P, Steinbeisser H. 1998. Pre-MBT patterning of early gene regulation in *Xenopus*: the role of the cortical rotation and mesoderm induction. Mech Dev 70:15–24.

Dingerkus G, Uhler LD. 1977. Enzyme clearing of Alcian blue stained whole small vertebrates for demonstration of cartilage. Stain Technol 52:229–232.

Ducy P, Zhang R, Geoffry V, Ridall AL, Karsenty G. 1997. Osf2/CBFa1: A transcriptional activator of osteoblast differentiation. Cell 89:747–754.

Eames FB, Sharpe PT, Helms JA. 2004. Hierarchy revealed in the specification of three skeletal fates by *Sox9* and *Runx2*. Dev Biol 274:188–200.

Enomoto H, Enomoto-Iwamoto M, Iwamoto M, Nomura S, Himeno M, Kitamura Y, Kishimoto T, Komori T. 2000. Cbfa1 is a positive regulatory factor in chondrocyte maturation. J Biol Chem 275: 8695–8702.

Enomoto H, Furuichi T, Zanma A, Yamana K, Yoshida C, Sumitani S, Yamamoto H, Enomoto-Iwamoto M, Iwamoto M, Komori T. 2004. Runx2 deficiency in chondrocytes causes adipogenic changes in vitro. J Cell Sci 117:417–425.

Enomoto-Iwamoto M, Enomoto H, Komori T, Iwamoto M. 2001. Participation of Cbfa1 in regulation of chondrocyte maturation. Osteoarthrit Cartil 9(Suppl A): S76–84.

Flores MV, Tsang VW, Hu W, Kalev-Zylinska M, Postlethwait J, Crosier P, Crosier K, Fisher S. 2004. Duplicate zebrafish *runx2* orthologues are expressed in developing skeletal elements. Gene Express Patterns 4:573–581.

Flores MV, Lam EY, Crosier P, Crosier K. 2006. A hierarchy of Runx transcription factors modulate the onset of chondrogenesis in craniofacial endochondral bones in zebrafish. Dev Dyn 235:3166–3176.

Fondon JW, 3rd, Garner HR. 2004. Molecular origins of rapid and continuous morphological evolution. Proc Natl Acad Sci USA 101:18058–18063.

Föske H. 1934. Das geruchsorgan von *Xenopus laevis*. [The olfactory organ in *Xenopus laevis*.] Zeit Anat Entwickl 103: 519–550.

Franceschi RT, Xiao G. 2003. Regulation of the osteoblast-specific transcription factor, Runx2: responsiveness to multiple signal transduction pathways. J Cell Biochem 88:446–454.

Glusman G, Kaur A, Hood L, Rowen L. 2004. An enigmatic fourth runt domain gene in the fugu genome: ancestral gene loss versus accelerated evolution. BMC Evol Biol 4:43–58.

Goldring MB, Tsuchimochi K, Ijiri K. 2006. The control of chondrogenesis. J Cell Biochem 97:33–44.

Gross JB, Hanken J. 2004. Use of fluorescent dextran conjugates as a long-term marker of osteogenic neural crest in frogs. Dev Dyn 230:100–106.

Hall BK. 2005. Bones and cartilage: developmental and evolutionary skeletal biology. New York: Elsevier Academic Press.

Harada H, Tagashira S, Fujiwara M, Ogawa S, Katsumata T, Yamaguchi A, Komori T, Nakatsuka M. 1999. Cbfa1 isoforms exert functional differences in osteoblast differentiation. J Biol Chem 274:6972–6978.

Inada M, Yasui T, Nomura S, Miyake S, Deguchi K, Himeno M, Sato M, Yamagiwa H, Kimura T, Yasui N, Ochi T, Endo N, Kitamura Y, Kishimoto T, Komori T. 1999. Maturational disturbance of chondrocytes in Cbfa1-deficient mice. Dev Dyn 214:279–290.

Ito Y. 2004. Oncogenic potential of the RUNX gene family: overview. Oncogene 23:4198–4208.

Iwamoto M, Kitagaki J, Tamamura Y, Gentilli C, Koyama E, Enomoto H, Komori T, Pacifici M, Enomoto-Iwamoto M. 2003. Runx2 expression and action in chondrocytes are regulated by retinoid signalling and parathyroid hormone-related peptide (PTHrP). Osteoarthrit Cartil 11:6–15.

Khokha MK, Yeh J, Grammer TC, Harland RM. 2005. Depletion of three BMP antagonists from Spemann's organizer leads to a catastrophic loss of dorsal structures. Dev Cell 8:401–411.

Kim IS, Otto F, Zabel B, Mundlos S. 1999. Regulation of chondrocyte differentiation by Cbfa-1. Mech Dev 80:159–170.

Komori T, Yagi H, Nomura S, Yamaguchi A, Sasaki K, Deguchi K, Y. S, Bronson R, Gao Y-H, Inada M, Sato M, Okamoto R, Kitamura Y, Yoshiki S, Kishimoto T. 1997. Targeted disruption of *cbfa1* results in a complete lack of bone formation owing to a maturational arrest of osteoblasts. Cell 89:7755–7764.

Kundu M, Javed A, Jeon J-P, Horner A, Shum L, Eckhaus M, Muenke M, Lian J, Yang Y, Nuckholls G, Stein G, Liu P. 2002. Cbfbeta interacts with Runx2 and has a critical role in bone development. Nat Gen 32:547–552.

Larrain J, Bachiller D, Lu B, Agius E, Piccolo S, De Robertis EM. 2000. BMP-binding modules in chordin: a model for signalling regulation in the extracellular space. Development 127:821–830.

Lengner CJ, Drissi H, Choi JY, van Wijnen AJ, Stein JL, Stein GS, Lian JB. 2002. Activation of the bone-related Runx2/Cbfa1 promoter in mesenchymal condensations and developing chondrocytes of the axial skeleton. Mech Dev 114:167–170.

Lengner CJ, Hassan MQ, Serra RW, Lepper C, van Wijnen AJ, Stein JL, Lian JB, Stein GS. 2005. Nkx3.2-mediated repression of Runx2 promotes chondrogenic differentiation. J Biol Chem 280:15872–15879.

Levanon D, Glusman G, Bettoun D, Ben-Asher E, Negreanu V, Bernstein Y, Harris-Cerruti C, Brenner O, Eilam R, Lotem J, Fainaru O, Goldenberg D, Pozner A, Woolf E, Xiao C, Yarmus M, Groner Y. 2003. Phylogenesis and regulated expression of the RUNT domain transcription factors RUNX1 and RUNX3. Blood Cells Mol Dis 30:161–163.

Lian JB, Balint E, Javed A, Drissi H, Vitti R, Quinlan EJ, Zhang L, Van Wijnen AJ, Stein JL, Speck N, Stein GS. 2003. Runx1/AML1 hematopoietic transcription factor contributes to skeletal development in vivo. J Cell Physiol 196:301–311.

Linsenmayer TF, Hendrix MJ. 1980. Monoclonal antibodies to connective tissue macromolecules: type II collagen. Biochem Biophys Res Commun 92:440–446.

Maddison WP, Maddison DR. 2005. Mesquite: a modular system for evolutionary analysis. Version 1.06. http://mesquiteproject.org

Mayor R, Morgan R, Sargent MG. 1995. Induction of the prospective neural crest of *Xenopus*. Development 121:767–777.

Mori-Akiyama Y, Akiyama H, Rowitch DH, de Crombrugghe B. 2003. Sox9 is required for determination of the chondrogenic cell lineage in the cranial neural crest. Proc Nat Acad Sci USA 100:9360–9365.

Moriishi T, Shibata Y, Tsukazaki T, Yamaguchi A. 2005. Expression profile of *Xenopus banded hedgehog*, a homolog of mouse Indian hedgehog, is related to the late development of endochondral ossification in *Xenopus laevis*. Biochem Biophys Res Commun 328:867–873.

Mundlos S, Otto F, Mundlos C, Molliken JB, Aylsworth AS, Albright S, Lindout D, Cole WG, Henn W, Knoll JH, Owen MJ, Mertelsmann R, Zabel BU, Olsen BR. 1997. Mutations involving the transcriptional factor CBF1 cause cleidocranial dysplasia. Cell 89:773–779.

Newman CS, Krieg PA. 1999. The *Xenopus* bagpipe-related homeobox gene zampogna is expressed in the pharyngeal endoderm and the visceral musculature of the midgut. Dev Genes Evol 209:132–134.

Nieuwkoop PD, Faber J. 1994. Normal table of *Xenopus laevis* (Daudin). New York: Garland Publishing. 252 p.

Otto F, Thornell A, Cromptom T, Denzell A, Gilmour K, Rosewell I, Stamp G, Beddington R, Mundlos S, Olsen B, Selby P, Owen M. 1997. Cbfa1, a candidate gene for cleidocranial dysplasia syndrome, is essential for osteoblast differentiation and bone development. Cell 89:765–771.

Pugener LA, Maglia AM, Trueb L. 2003. Revisiting the contribution of larval characters to an analysis of phylogenetic relatioinships of basal anurans. Zool J Linnean Soc 139:129–155.

Rennert J, Coffman JA, Mushegian AR, Robertson AJ. 2003. The evolution of Runx genes I. A comparative study of sequences from phylogenetically diverse model organisms. BMC Evol Biol 3:4.

Roček Z. 2003. Larval development and evolutionary origin of the anuran skull. In: Heatwole H, Davies M, editors. Amphibian biology, Vol. 5: osteology. Chipping Norton, Australia: Surrey Beatty and Sons. p 1877–1995.

Roček Z, Vesley M. 1989. Development of the ethmoidal structures of the endocranium in the anuran *Pipa pipa*. J Morphol 200:301–309.

Sadaghiani B, Thièbaud CH. 1987. Neural crest development in the *Xenopus laevis* embryo, studied by interspecific transplantation and scanning electron microscopy. Dev Biol 124:91–110.

Schreiber A, Das B, Huang H, Marsh-Armstrong N, Brown D. 2001. Diverse developmental programs of *Xenopus laevis* metamorphosis are inhibited by a dominant negative thyroid hormone receptor. Proc Natl Acad Sci USA 98:10739–10744.

Sedra S, Michael M. 1957. The development of the skull, visceral arches, larynx and visceral muscles of the South African clawed toad, *Xenopus laevis* (Daudin) during the process of metamorphosis (from stage 55 to stage 66). Verh Kon Nederlandse Akad afg Natuurkunde ser 2:1–80.

Seufert DW, Hanken J, Klymkowsky MW. 1994. Type II collagen distribution during cranial development in *Xenopus laevis*. Anat Embryol 189:81–89.

Shibata S, Suda N, Yoda S, Fukuoka H, Ohyama K, Yamashita Y, Komori T. 2004. Runx2-deficient mice lack mandibular condylar cartilage and have deformed Meckel's cartilage. Anat Embryol (Berl) 208:273–280.

Shibata S, Suda N, Suzuki S, Fukuoka H, Yamashita Y. 2006. An in situ hybridization study of Runx2, Osterix, and Sox9 at the onset of condylar cartilage formation in fetal mouse mandible. J Anat 208:169–177.

Sive HL, Grainger RM, Harland RM. 2000. Early development of *Xenopus laevis*. Cold Spring Harbor, NY: Cold Spring Harbor Laboratory Press.

Smith N, Dong Y, Lian JB, Pratap J, Kingsley PD, van Wijnen AJ, Stein JL, Schwarz EM, O'Keefe RJ, Stein GS, Drissi MH. 2005. Overlapping expression of Runx1(Cbfa2) and Runx2(Cbfa1) transcription factors supports cooperative induction of skeletal development. J Cell Physiol 203:133–143.

Sokol OM. 1975. The phylogeny of anuran larvae: a new look. Copeia 1975:1-24.

Sokol OM. 1977. The free swimming *Pipa* larvae with a review of pipid phylogeny (Anura: Pipidae). J Morphol 154:357–426.

Speck N, Dzierzak E. 2001. Runx1 (Aml1) and CBFB: genes required for the development of all definitive hematopoetic lineages. In: Ravid K, Licht J, editors. Transcription factors: normal and malignant development of blood cells. Hoboken, NJ: Wiley-Liss, Inc.

Spemann H. 1898. Über die Entwicklung der Tuba Eustachii und des Kopfskelletes von *Rana temporaria*. [On the development of the eustachian tube and the head skeleton of *Rana temporaria*.] Zool J 11:389–416.

Spokony RF, Aoki Y, Saint-Germain N, Magner-Fink E, Saint-Jeannet JP. 2002. The transcription factor Sox9 is required for cranial neural crest development in *Xenopus*. Development 129:421–432.

Stock M, Otto F. 2005. Control of RUNX2 isoform expression: the role of promoters and enhancers. J Cell Biochem 95:506–517.

Svensson ME, Haas A. 2005. Evolutionary innovation in the vertebrate jaw: A derived morphology in anuran tadpoles and its possible developmental origin. Bioessays 27:526–532.

Swart C, de Sá R. 1999. The chondrocranium of the Mexican burrowing toad, *Rhinophrynus dorsalis*. J Herpetol 33:23–28.

Thirunavukkarusu K, Mahajan M, McLarren K, Stifani S, Karsenty G. 1998. Two domains unique to the osteoblast-specific transcription factor Osf2/Cbfa1 contribute to its transactivation function and its inability to heterodimerize with Cbfbeta. Mol Cell Biol 18:4197–4208.

Trueb L, Hanken J. 1992. Skeletal development in *Xenopus laevis* (Anura: Pipidae). J Morphol 214:1–41.

Ueta C, Iwamoto M, Kanatani N, Yoshida C, Liu Y, Enomoto-Iwamoto M, Ohmori T, Enomoto H, Nakata K, Takada K, Kurisu K, Komori T. 2001. Skeletal malformations caused by overexpression of Cbfa1 or its dominant negative form in chondrocytes. J Cell Biol 153:87–100.

van der Meulen T, Kranenbarg S, Schipper H, Samallo J, van Leeuwen JL, Franssen H. 2005. Identification and characterisation of two runx2 homologues in zebrafish with different expression patterns. Biochim Biophys Acta 1729:105–117.

Wang W, Wang YG, Reginato AM, Glotzer DJ, Fukai N, Plotkina S, Karsenty G, Olsen BR. 2004. Groucho homologue Grg5 interacts with the transcription factor Runx2-Cbfa1 and modulates its activity during postnatal growth in mice. Dev Biol 270:364–381.

Wang Y, Belflower RM, Dong YF, Schwarz EM, O'Keefe RJ, Drissi H. 2005. Runx1/AML1/Cbfa2 mediates onset of mesenchymal cell differentiation toward chondrogenesis. J Bone Miner Res 20:1624–1636.

Xiao ZS, Simpson LG, Quarles LD. 2003. IRES-dependent translational control of Cbfa1/Runx2 expression. J Cell Biochem 88:493–505.

Yamashiro T, Aberg T, Laevanon D, Groner Y, Thesleff I. 2002. Expression of *Runx1, -2,* and *-3* during tooth, palate and craniofacial bone development. Mech Dev 119S:S107–S110.